Structure of excited states of ^{10}Be studied with antisymmetrized molecular dynamics

Y. Kanada-En'yo
Institute of Particle and Nuclear Studies, High Energy Accelerator Research Organization, 3-2-1 Midori-cho Tanashi, Tokyo 188-8501, Japan

H. Horiuchi and A. Doté
Department of Physics, Kyoto University, Kyoto 606-01, Japan
(Received 21 May 1999; published 27 October 1999)

We study the structure of excited states of ^{10}Be with the method of variation after spin-parity projection in the framework of antisymmetrized molecular dynamics. Present calculations describe many excited states and reproduce the experimental data of $E2$ and $E1$ transitions and the new data of the β transition strength successfully. We include systematic discussions on the moleculelike structures of light unstable nuclei and the important role of the valence neutrons based on the results obtained with the framework which is free from such model assumptions as the existence of inert cores and clusters. [S0556-2813(99)05011-6]

PACS number(s): 21.10.Pc, 21.60.−n, 27.20.+n, 02.70.Ns

I. INTRODUCTION

Owing to the radioactive nuclear beams, the data of unstable nuclei are increasing rapidly. Recently the structure of excited states as well as the ground states are very attractive in the study of unstable nuclei. In the light nuclear region, one of the important subjects has been the clustering features. The clustering structures of the ground states are already well known to be developed in some light ordinary nuclei such as ^{7}Li, ^{8}Be, and ^{20}Ne. In the studies of the light unstable nuclei the clustering structures were predicted also in the very neutron-rich nuclei [1–6]. It is natural that various moleculelike states may appear in the excited states of light unstable nuclei because the excitation due to relative motion between clusters is important in the light nuclear region. The clustering structure must be one of the important aspects in understanding the exotic features of the unstable nuclei. However, there remain many mysterious problems of clustering development and the role of valence nucleons in the unstable nuclei. Our aim is to make a systematic study of structure change with the increase of the excitation energy. We find new features of unstable nuclei such as exotic shapes and moleculelike structures in the excited states and try to understand the mechanism of the various structures.

^{10}Be, one of the challenges in the study of light unstable nuclei, has been investigated experimentally in such reactions as transfer and pick-up, as well as in the experiments with the technique of unstable nuclear beams. Recent experiments of the charge exchange reactions ^{10}B(^{3}He,t)^{10}Be [7] let us know the strength of the Gamow-Teller transitions to the excited states of ^{10}Be. These new data of β transition strength which are deduced from the cross sections at the forward angle are very helpful for studying the structure of the excited states. The structure of ^{10}Be was and is studied also theoretically by microscopic calculations, for example, shell models [8,9], cluster models [1,5,6], Hartree-Fock [3], and antisymmetrized molecular dynamics [2,4].

As for the shell-model studies on p-shell nuclei, calculations with the inclusion of the $2\hbar\omega$ excitation with empirical effective interactions were successful in fitting a wide range of the data for energy levels [8,9]. As far as the low-lying states go, the properties of the structure can be described [10], however, the model space is not large enough yet to study the structures of such states with the developed clustering which may appear in the excited states of light nuclei. For the large-basis shell model it is not easy to obtain the the empirical effective interactions. In the calculations with $4\hbar\omega$ model space with a microscopic effective interaction [11], the level structure in ^{10}Be is not well reproduced.

Many states of Be isotopes are understood in terms of 2α clustering structures. In the theoretical research on the structure of the ground states of Be isotopes such as Ref. [2], it was found that the developed 2α clustering structure in ^{8}Be weakens in ^{10}Be because of the excess two neutrons. As for the excited states of ^{10}Be, the previous calculations [12] with the simplest version (variation after parity projection) of antisymmetrized molecular dynamics (AMD) predicted that the largely deformed states with the $2\alpha+2n$ clustering structure construct a rotational band $K^{\pi}=1^{-}$ in the low-energy region which is supported by the experimental energy levels.

The problem of the abnormal spin parity $1/2^{+}$ in the ground state of ^{11}Be is considered to have a close relation with the deformed non-normal parity states of ^{10}Be. In the simple shell-model consideration the normal parity of ^{11}Be is negative because of the valence neutron in the $p_{1/2}$ shell, however, the ground states is known to be $J^{\pi}=1/2^{+}$. It is suggested that one of the reasons for the parity inversion in ^{11}Be is the energy gain of the $sd_{1/2}$ mixing orbit in the prolately deformed system due to developed clustering. The $sd_{1/2}$ orbit of neutrons in neutron-rich Be isotopes is interesting and essential to understanding the structure of light neutron-rich nuclei and is easily connected with the deformed structure of the non-normal parity states of ^{10}Be. Furthermore, it is natural that the negative parity band due to the deformed states of ^{10}Be makes us imagine a corresponding positive parity band constructed by the analogous deformed intrinsic state where the neutrons in the $sd_{1/2}$ orbit play important roles.

Recently Von Oertzen proposed a dimer model [13] to describe the excited states of Be and B isotopes systemati-

cally. In the model, he assumed 2α clusters and the surrounding nucleons in molecular orbits which are similar to the σ and π orbits of electrons in the molecule. The neutron-rich Be nuclei can be written by 2α and neutrons which occupy the moleculelike σ and π orbits. This idea is helpful for understanding the level structure of many excited states of ^{9}Be and ^{10}Be and for studying the mechanism of the deformation of Be isotopes.

Doté *et al.* studied Be isotopes by microscopic calculations with the simplest version of AMD under a constraint on the deformation parameter [4]. They analyzed the single-particle orbits of the valence neutrons and found the importance of molecular orbits. It was found that in the negative parity state of ^{10}Be the main component of the valence neutrons is the positive parity orbit which seems to be the σ orbit in terms of the dimer model. They tried to represent the excited 0_2^+ state of ^{10}Be by constructing $2p$-$2h$ states using the wave function of the negative parity state which is considered to be $1p$-$1h$ state. Comparing the optimum deformation parameters for three states 0_1^+, 1^-, and 0_2^+, they found that the intrinsic deformation is larger in 1^- than 0_1^+ and largest in 0_2^+. The results are consistent with those predicted by Von Oertzen. They calculated excited states 0_2^+ of ^{10}Be without assuming any cluster cores and confirmed that the 2α cluster cores may exist in the excited states. However, since the total-angular-momentum projection was not done microscopically, the discussion did not go beyond the intrinsic system and it is not easy to study other excited states. They have not mentioned the data such as $E1$, $E2$, and β transitions which are important in the study of excited states.

^{10}Be has been studied with other microscopic models such as multicluster models [6], AMD+GCM (generator coordinate method) [5], and the parity-projected Hartree-Fock (HF) calculations [3]. In the former two methods the existence of α clusters was assumed. In the last work with parity-projected HF calculations they assumed the excited 0_2^+ state to be a $2p$-$2h$ state by choosing the positive parity eigenstate for the valence two neutrons. In the work with HF calculations, the analysis was limited in the intrinsic system and it is not easy to study the higher excited states.

Our aim is to make systematic studies on the structure of many excited states of the light unstable nuclei with a microscopic model which is free from such assumptions as the inert cores, the existence of clusters, and the particle-hole configurations. For this aim we adopt a method of antisymmetrized molecular dynamics (AMD). AMD has already proven to be a very useful theoretical approach for the structure of the light nuclei [2,4,14,15]. In the AMD framework basis wave functions of the system are written by Slater determinants where the spatial part of each single-particle wave function is a Gaussian wave packet. In the previous works on the structure of Li, Be, and B isotopes [2], we applied the simplest version of AMD in which the energy variation is done after the parity projection but before the total-angular momentum projection. It was found that the structure of the ground state changes rapidly between the shell-model-like structure and the clustering structure as the neutron number increases up to the neutron-drip line. The AMD calculations succeeded in reproducing well the experimental data for electromagnetic properties such as the magnetic dipole moments and the electric quadrupole moments. This is due to the flexibility of the AMD wave function which can represent the clustering structures of light unstable nuclei without assuming any inert cores and clusters.

In the present paper, we study the structure of the excited states of ^{10}Be by performing variational calculations after the spin-parity projection with finite-range interactions in the framework of AMD. For higher states, AMD wave functions are superposed so as to be orthogonal to the lower states. The AMD approach of the variation after spin-parity projection (VAP) has been already found to be advantageous for the study of excited states of the light nuclei and very useful for describing various moleculelike structures [15,16]. We do not rely on any assumptions such as the inert cores, the single-particle orbits in the mean field, and the existence of clusters. By microscopic calculations of the expectation values of the corresponding operators, we can acquire the theoretical values of $E2$, $E1$, and β transitions which is the valuable information of the excited states to be compared directly with the experimental data.

In Sec. II, we explain the formulation of AMD for the study of the nuclear structure of excited states. The effective interactions are described in Sec. III, and the results are presented in Sec. IV comparing with the experimental data. In Sec. V, detailed discussions on the structures and on the mechanism of the development of moleculelike structures are made. Finally, a summary is given in Sec. VI.

II. FORMULATION

In this section we explain the formulation of AMD for the study of the nuclear structure of the excited states.

A. Wave function

The wave function of a system is written by AMD wave functions as

$$\Phi = c\Phi_{\mathrm{AMD}} + c'\Phi'_{\mathrm{AMD}} + \cdots . \tag{1}$$

An AMD wave function of a nucleus with mass number A is a Slater determinant of Gaussian wave packets:

$$\Phi_{\mathrm{AMD}}(\mathbf{Z}) = \frac{1}{\sqrt{A!}}\mathcal{A}\{\varphi_1, \varphi_2, \ldots, \varphi_A\}, \tag{2}$$

$$\varphi_i = \phi_{\mathbf{X}_i}\chi_{\xi_i}\tau_i : \begin{cases} \phi_{\mathbf{X}_i}(\mathbf{r}_j) \propto \exp\left[-\nu\left(\mathbf{r}_j - \dfrac{\mathbf{X}_i}{\sqrt{\nu}}\right)^2\right], \\ \chi_{\xi_i} = \begin{pmatrix} \dfrac{1}{2} + \xi_i \\ \dfrac{1}{2} - \xi_i \end{pmatrix}, \end{cases} \tag{3}$$

where the ith single-particle wave function φ_i is a product of the spatial wave function, the intrinsic spin function and the isospin function. The spatial part ϕ_{X_i} is presented by com-

plex parameters X_{1i}, X_{2i}, X_{3i}, χ_{ξ_i} is the intrinsic spin function parametrized by ξ_i, and τ_i is the isospin function which is fixed to be up (proton) or down (neutron) in the present calculations. Thus an AMD wave function is parametrized by a set of complex parameters $\mathbf{Z} \equiv \{X_{ni}, \xi_i\}$ ($n=1,3$ and $i=1,A$), where the $\mathbf{X}_i$'s indicate the centers of Gaussians of the spatial part and the ξ_i's are the parameters for the directions of the intrinsic spins.

If we consider a parity eigenstate projected from an AMD wave function, the total wave function consists of two Slater determinants,

$$\Phi(\mathbf{Z}) = (1 \pm P)\Phi_{\mathrm{AMD}}(\mathbf{Z}), \tag{4}$$

where P is a parity projection operator. In the case of a total-angular momentum eigenstate, the wave function of a system is represented by the integral of the rotated states,

$$\Phi(\mathbf{Z}) = P^{J}_{MK'}\Phi_{\mathrm{AMD}}(\mathbf{Z}) = \int d\Omega D^{J*}_{MK'}(\Omega) R(\Omega)\Phi_{\mathrm{AMD}}(\mathbf{Z}), \tag{5}$$

for which the expectation values of operators are numerically calculated by a summation of mesh points on the Euler angles Ω.

In principal, the total wave function can be the superposition of independent AMD wave functions. In order to construct higher excited states we consider superposition of the spin-parity-projected AMD wave functions $P^{J^\pm}_{MK'}\Phi_{\mathrm{AMD}}$,

$$\Phi = cP^{J^\pm}_{MK'}\Phi_{\mathrm{AMD}}(\mathbf{Z}) + c' P^{J^\pm}_{MK'}\Phi_{\mathrm{AMD}}(\mathbf{Z}') + \cdots. \tag{6}$$

The detail is mentioned later in Sec. II D.

B. Energy variation

We make variational calculations to find the state which minimizes the energy of the system:

$$\frac{\langle \Phi | H | \Phi \rangle}{\langle \Phi | \Phi \rangle}, \tag{7}$$

by the method of frictional cooling. Regarding the frictional cooling method in AMD, the reader is referred to [2,14]. For the wave function $\Phi(\mathbf{Z})$ parametrized by $\mathbf{Z}$, the time development of the parameters is given by the frictional cooling equations

$$\frac{dX_{nk}}{dt} = (\lambda + i\mu)\frac{1}{i\hbar}\frac{\partial}{\partial X^*_{nk}}\frac{\langle \Phi(\mathbf{Z})|H|\Phi(\mathbf{Z})\rangle}{\langle \Phi(\mathbf{Z})|\Phi(\mathbf{Z})\rangle}, \quad (n=1,3 \quad k=1,A), \tag{8}$$

$$\frac{d\xi_k}{dt} = (\lambda + i\mu)\frac{1}{i\hbar}\frac{\partial}{\partial \xi^*_k}\frac{\langle \Phi(\mathbf{Z})|H|\Phi(\mathbf{Z})\rangle}{\langle \Phi(\mathbf{Z})|\Phi(\mathbf{Z})\rangle}, \quad (k=1,A) \tag{9}$$

with arbitrary real numbers λ and $\mu < 0$. It is easily proved that the energy of the system decreases with time. After sufficient time steps of cooling, the parameters for the wave function of the minimum-energy state are obtained.

C. Lowest $J^\pm$ states

In order to obtain the wave function for the lowest $J^\pm$ state, we perform the energy variation for the spin-parity eigenstates projected from an AMD wave function. In this case the trial function is $\Phi = P^{J^\pm}_{MK'}\Phi_{\mathrm{AMD}}(\mathbf{Z})$. In the previous works [2] with the simplest version of AMD for the study of nuclear structure, the approach was a variation after only the parity projection but a variation before the total spin projection (VBP). In the present paper, the approach is a variation after the spin-parity projection (VAP). First we make VBP calculations to prepare an initial wave function $\Phi_{\mathrm{AMD}}(\mathbf{Z}_{\mathrm{init}})$ for the VAP calculations. We choose an appropriate K' quantum that gives the minimum diagonal energy of the spin-parity eigenstate

$$\langle P^{J^\pm}_{MK'}\Phi_{\mathrm{AMD}}(\mathbf{Z}_{\mathrm{init}})|H|P^{J^\pm}_{MK'}\Phi_{\mathrm{AMD}}(\mathbf{Z}_{\mathrm{init}})\rangle / \langle P^{J^\pm}_{MK'}(\mathbf{Z}_{\mathrm{init}})|P^{J^\pm}_{MK'}(\mathbf{Z}_{\mathrm{init}})\rangle,$$

where K' is the component of the total-angular momentum along the approximately principal axis in the intrinsic system. For each spin parity $J^\pm$, we perform VAP calculations for

$$\langle P^{J^\pm}_{MK'}\Phi_{\mathrm{AMD}}(\mathbf{Z})\,|H|\,P^{J^\pm}_{MK'}\Phi_{\mathrm{AMD}}(\mathbf{Z})\rangle / \langle P^{J^\pm}_{MK'}(\mathbf{Z})\,|P^{J^\pm}_{MK'}(\mathbf{Z})\rangle$$

with the adopted K' quantum from the initial state. In the VAP procedure, the principal z axis of the intrinsic deformation is not assumed to be equal with the third axis of Euler angle in the total-angular momentum projection. In general the principal z axis is automatically determined in the energy variation, that is to say that the obtained state $P^{J^\pm}_{MK'}\Phi_{\mathrm{AMD}}$ by VAP with a given $K' = \langle J_3 \rangle$ can be the state with so-called K mixing in terms of the intrinsic deformation where the $K = \langle J_z \rangle$ quantum is defined on the principal axis. In many cases, the z axis determined in the VAP calculation is found to be approximate to the third axis. It means that the obtained states do not contain K mixing so much, and K' is considered to be the approximate K quantum for the principal axis. The excited $J^\pm$ states in the band $K^\pi = K''^\pm$ other than the K' quantum of the lower $J^\pm$ states are obtained by VAP calculations for $P^{J^\pm}_{MK''}\Phi_{\mathrm{AMD}}$ under the constraint on the principal axis z as equal to the third axis.

D. Higher excited states

As mentioned above, with the VAP calculation for $\Phi(\mathbf{Z}) = P^{J^\pm}_{MK'}\Phi_{\mathrm{AMD}}(\mathbf{Z})$ of the $J^\pm$ eigenstate with K', we obtain the set of parameters $\mathbf{Z} = \mathbf{Z}^{J^\pm}_1$ which present the wave function for the first $J^\pm$ state. To search for the parameters $\mathbf{Z}$ for the higher excited $J^\pm$ states in the nth $K^\pi = K'^\pm$ band, the wave functions are superposed to be orthogonal to the lower states as follows. The parameters $\mathbf{Z}^{J^\pm}_n$ for the nth $J^\pm$ state are reached by varying the energy of the orthogonal component to the lower states:

$$\Phi(\mathbf{Z}) = P^{J^\pm}_{MK'}\Phi_{\rm AMD}(\mathbf{Z}) - \sum_{k=1}^{n-1} \frac{\langle P^{J^\pm}_{MK'}\Phi_{\rm AMD}(\mathbf{Z}^{J^\pm}_k)|P^{J^\pm}_{MK'}\Phi_{\rm AMD}(\mathbf{Z})\rangle}{\langle P^{J^\pm}_{MK'}\Phi_{\rm AMD}(\mathbf{Z}^{J^\pm}_k)|P^{J^\pm}_{MK'}\Phi_{\rm AMD}(\mathbf{Z}^{J^\pm}_k)\rangle} \times P^{J^\pm}_{MK'}\Phi_{\rm AMD}(\mathbf{Z}^{J^\pm}_k). \quad (10)$$

E. Expectation values

After VAP calculations for various $J^\pm_n$ states, the intrinsic states $\Phi^1_{\rm AMD}, \Phi^2_{\rm AMD}, \ldots, \Phi^m_{\rm AMD}$, which approximately correspond to the $J^\pm_n$ states, are obtained as much as the number of the calculated levels. Finally we determine the wave functions for the $J^\pm_n$ states by diagonalizing the Hamiltonian matrix $\langle P^{J^\pm}_{MK'}\Phi^i_{\rm AMD}|H|P^{J^\pm}_{MK''}\Phi^j_{\rm AMD}\rangle$ and the norm matrix $\langle P^{J^\pm}_{MK'}\Phi^i_{\rm AMD}|P^{J^\pm}_{MK''}\Phi^j_{\rm AMD}\rangle$ simultaneously with regard to (i,j) for all the intrinsic states and (K',K''). In comparison with the experimental data such as energy levels and $E2$ transitions, the theoretical values are calculated with the final states after diagonalization.

III. INTERACTIONS

The adopted interaction for the central force is case 3 of the MV1 force [17], which contains a zero-range three-body force $V^{(3)}$ as a density-dependent term in addition to the two-body interaction $V^{(2)}$ of the modified Volkov force,

$$V_{DD} = V^{(2)} + V^{(3)}, \quad (11)$$

$$V^{(2)} = (1 - m + bP_\sigma - hP_\tau - mP_\sigma P_\tau)\left\{ V_A \exp\left[-\left(\frac{r}{r_A}\right)^2 \right] + V_R \exp\left[-\left(\frac{r}{r_R}\right)^2 \right] \right\}, \quad (12)$$

$$V_A = -83.34 \ \text{MeV}, \quad r_A = 1.60 \ \text{fm},$$

$$V_R = 99.86 \ \text{MeV}, \quad r_R = 0.82 \ \text{fm}, \quad (13)$$

$$V^{(3)} = v^{(3)}\delta(\mathbf{r}_1 - \mathbf{r}_2)\delta(\mathbf{r}_1 - \mathbf{r}_3), \quad v^{(3)} = 5000 \ \text{MeV fm}^6, \quad (14)$$

where P_σ and P_τ stand for the spin and isospin exchange operators, respectively. As for the two-body spin-orbit force V_{LS}, we adopted the G3RS force [18] as follows:

$$V_{LS} = \{u_I \exp(-\kappa_I r^2) + u_{II} \exp(-\kappa_{II} r^2)\} \frac{(1+P_\sigma)}{2} \frac{(1+P_\tau)}{2} \mathbf{L}\cdot(\mathbf{S_1}+\mathbf{S_2}), \quad (15)$$

$$\kappa_I = 5.0 \ \text{fm}^{-2}, \quad \kappa_{II} = 2.778 \ \text{fm}^{-2}. \quad (16)$$

The Coulomb interaction $V_{\rm C}$ is approximated by a sum of seven Gaussians.

We treat the resonance states within a bound-state approximation by situating an artificial barrier $\mathcal{E}_{\rm barr}$. In the variational calculation we variate the modified energy $\mathcal{E}' = \mathcal{E} + \mathcal{E}_{\rm barr}$ with the additional artificial energy $\mathcal{E}_{\rm barr}$ instead of $\mathcal{E} \equiv \langle\Phi|H|\Phi\rangle/\langle\Phi|\Phi\rangle$, where H is the Hamiltonian operator; $H = T + V_{DD} + V_{LS} + V_{\rm C}$. For the barrier in the present calculations we adopt a function of the real part of the centers $\mathbf{X}_i$ of the single-particle wave functions as follows:

$$\mathcal{E}_{\rm barr} = V_W \sum_{i=1}^{A} \exp\left[-2\nu \left(r_a - \frac{|{\rm Re}[\mathbf{X}_i]|}{\sqrt{\nu}} \right)^2 \right], \quad (17)$$

$$r_a = r_0(2 \ {\rm Max}[Z,N])^{1/3} + b, \quad (18)$$

$$V_W = 2.5 \ \text{MeV}, \quad r_0 = 1.2 \ \text{fm}, \quad b = \sqrt{\frac{3}{2\nu}} \ \text{fm}, \quad (19)$$

where Z and N are proton and neutron numbers, respectively. We put the artificial barrier only in the variational calculation, but do not put the barrier in the diagonalization of the Hamiltonian matrix after VAP calculations. In the present calculations of ^{10}Be, the artificial energies due to the barrier are found to be a few hundreds keV at most and have no significant effect on the results in most levels.

IV. RESULTS

The structure of the excited states of ^{10}Be is studied with the VAP calculations in the framework of AMD. In this section we display the theoretical results of the excitation energies, $E2$, $E1$, and β transitions which can be directly compared with the experimental data. The detail of the structures is discussed in the next section. The adopted parameters of the interactions are $m = 0.62$, $b = h = 0$ for the Majorana, Bertlett, and Heisenberg terms of the central force and the strength of the spin-orbit force $u_I = -u_{II} = 3000$ MeV [case (1)]. Trying another set of parameters, case (2) with $m = 0.65$, $b = h = 0$ and $u_I = -u_{II} = 3700$ MeV, we did not find significant differences in the results. The set of parameters of case (1) is the one adopted in the work on ^{12}C [15]. On the other hand, the VAP calculations with the set of interactions of case (2) reproduce the parity inversion of the ground state of ^{11}Be. The optimum width parameters ν of wave packets are chosen to be 0.17 fm^{-2} for case (1) and 0.19 fm^{-2} for case (2) which give the minimum energies in VBP calculations of ^{10}Be. The resonance states are treated within a bound-state approximation by situating an artificial barrier out of the surface as mentioned in Sec. III.

The lowest $J^\pm$ states are obtained by VAP calculations for $P^{J^\pm}_{MK'}\Phi_{\rm AMD}$ with $(J^\pm,K') = (0^+,0)$, $(2^+,0)$, $(3^+,+2)$, $(4^+,0)$, $(1^-,-1)$, $(2^-,-1)$, $(3^-,-1)$, $(4^-,-1)$. Considering the 0^+_2 state to be a 0^+ state in the second $K^\pi = 0^+$ band, the 0^+_2 state is calculated by VAP as the higher excited state orthogonal to the lowest 0^+_1 state as explained in the Sec. II D. That is to say that the 0^+_2 state is obtained by VAP for $\Phi(\mathbf{Z})$ in Eq. (10) with $(J^\pm,K',n) = (0^+,0,2)$. In the case of higher 2^+ states, we use the constraint that the approximately principal z axis of the intrinsic deformation is equal to the third axis of the Euler angle in the total-spin projection. According to VBP calculations the second 2^+ state is described as the band head of the lowest $K^\pi = 2^+$ band.

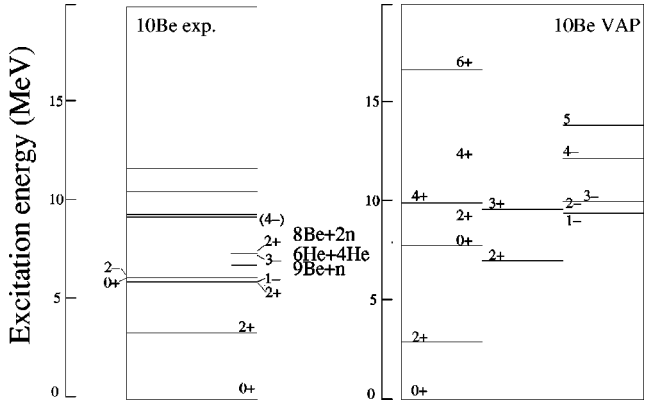

FIG. 1. Excitation energies of the levels in ^{10}Be. Theoretical results are calculated by the diagonalization of the states obtained with VAP by using the interaction case (1).

Therefore, we construct the state 2_2^+ by choosing $(J^\pm,K')$ of $P^{J\pm}_{MK'}\Phi_{\rm AMD}$ as $(J^\pm,K')=(2^+,+2)$ under the constraint on the principal z axis which keeps the approximate orthogonality to the lowest 2^+ state with $(J^\pm,K')=(2^+,0)$. The third 2_3^+ state is easily conjectured to be a 2^+ state in the second $K^\pi=0_2^+$ band, like the 0_2^+ state. We obtain the 2_3^+ state by VAP for $\Phi(\mathbf{Z})$ in Eq. (10) with $(J^\pm,K',n)=(2^+,0,2)$ in the same way as the 0_2^+ state, under the constraint on the principal z axis mentioned above. It means that the orthogonal condition to 2_1^+ is kept by superposing two wave functions as described in Sec. II D, while the orthogonality to 2_2^+ $(K^\pi=2^+)$ is taken into account by choosing different K quantum $K'=0$.

The binding energy obtained with case (1) interactions is 61.1 MeV, and the one with case (2) is 61.3 MeV. The excitation energies of the results are displayed in Fig. 1. By diagonalization of the Hamiltonian matrix the excited states 4_2^+, 6^+ are found in the rotational band the $K^\pi=0_2^+$ and the 5^- state is seen in the $K^\pi=1^-$ band. Comparing with the experimental data, the level structure is well reproduced by theory. Although it is difficult to estimate the width of resonance within the present framework, the theoretical results suggest the existence of 3^+, 4^+, 6^+, and 5^- states which are not experimentally identified yet. The excited levels can be roughly classified as the rotational bands $K^\pi=0_1^+$, 2^+, 0_2^+, and 1^- which consist of $(0_1^+, 2_1^+, 4_1^+)$, $(2_2^+, 3_1^+)$, $(0_2^+, 2_3^+, 4_2^+, 6_1^+)$, and $(1^-, 2^-, 3^-, 4^-, 5^-)$, respectively. The intrinsic structures of these rotational bands are discussed in detail in the next section.

The data of the transition strength are of great help to investigate the structures of the excited states. The results with the interaction case (1) and the experimental data of $E2$ and $E1$ transition strength are presented in Table I. The theoretical values agree well with the experimental data. The strength $B(E2)$ for ^{10}C;$2_1^+\rightarrow 0_1^+$ is simply calculated by the wave function of ^{10}C supposed to be mirror symmetric with ^{10}Be. The present result for the $E2$ strength of ^{10}C;$2_1^+\rightarrow 0_1^+$ is better than the work with simple AMD calculations [19] mainly due to the superposition of many wave functions by diagonalization. As the values with a shell model, $(0+2)\hbar\omega$ shell-model calculations with effective charges $e_\pi=1.05e, e_\nu=0.05e$ from Ref. [10] are also listed. Also the shell-model calculations reproduce the experimental data of the $E2$ properties of low-lying levels.

The strength of the β decays of Gamow-Teller (GT)-type transitions can be deduced from the cross sections at the 0° forward angle of the charge exchange reactions which have been measured recently [7]. These new data for the Gamow-Teller-type β transitions are very useful probes to discuss the structures of the excited states of unstable nuclei. Table II shows the values of B(GT). The experimental values for the β transitions from ^{10}B$(3+)$ to ^{10}Be* are deduced from the data of the reaction ^{10}B$(t,^3$He$)^{10}$Be. As for the theoretical values, the wave functions for the neighbor nucleus ^{10}B are calculated with VAP where $(J^\pm,K')$ are chosen to be $(3^+,-3)$ for the ground 3_1^+ state and $(1^+,-1)$ for the 1_1^+ state. ^{10}Be and ^{10}B are calculated with case (1) and (2) interactions. The theoretical values reasonably match the experimental data. Since the data for ^{10}B$(3^+)\rightarrow{}^{10}$Be(9.4 MeV) correspond well to the theoretical value of ^{10}B$(3^+)\rightarrow{}^{10}$Be(3_1^+), it is natural to consider the excited level of ^{10}Be at 9.4 MeV as the 3_1^+ state. The strength of these GT transitions from ^{10}B(3^+) is governed by the configuration of the ground state of ^{10}B which is understood as the state 3^+ with $|K|=3$ in the p shell in the simple shell-model limit. It is natural that the transitions to 2_2^+ and 3_1^+ states in the $K^\pi=2^+$ bands of ^{10}Be are strong while the transitions to the states in the $K^\pi=0^+$ bands are weaker. The strength is not so sensitive to the interactions except for the decay ^{10}B$(3^+)\rightarrow{}^{10}$Be(2_1^+). The results of the GT transition ^{10}B$(3^+)\rightarrow{}^{10}$Be(2_1^+) with case (1) and case (2) interactions underestimate the experimental data. It is because the $K=2$ component hardly mixes in the 2_1^+ state of ^{10}Be in the case

TABLE I. $E2$ and $E1$ transition strength. The theoretical results of AMD with the interaction case (1) are compared with the experimental data [20]. The shell model calculations are quoted from the work with the $(0+2)\hbar\omega$ shell model in Ref. [10].

Transitions	Mult.	Expt.	Present AMD	Shell model
^{10}Be;$2_1^+\rightarrow 0_1^+$	$E2$	10.5 ± 1.1 (e fm^2)	11 (e fm^2)	16.26 (e fm^2)
^{10}Be; $0_2^+\rightarrow 2_1^+$	$E2$	3.3 ± 2.0 (e fm^2)	0.6 (e fm^2)	7.20 (e fm^2)
^{10}Be; $0_2^+\rightarrow 1_1^-$	$E1$	$1.3\pm0.6\times10^{-2}$ (e fm)	0.6×10^{-2}(e fm)	
^{10}C;$2_1^+\rightarrow 0_1^+$	$E2$	12.3 ± 2.0 (e fm^2)	9 (e fm^2)	15.22 (e fm^2)

of these interactions. On the other hand, a larger value 0.27 for $^{10}\mathrm{B}(3^+)\rightarrow{}^{10}\mathrm{Be}(2_1^+)$ is calculated with another set of interactions; Volkov No. 2 ($m=0.38, b=0,2, h=-0.4$) + G3RS($u_I=-u_{II}=1600$ MeV) + Coulomb, in which the 2_1^+ state in the $K^\pi=0_1^+$ band contains the mixing of the $K=2$ component. It is predicted that the $B(\mathrm{GT})$ for $^{10}\mathrm{B}(3^+)\rightarrow{}^{10}\mathrm{Be}(2_3^+)$ is small because $^{10}\mathrm{Be}(2_3^+)$ is the state in the $K^\pi=0_2^+$ band which is constructed by the linear structure with the developed clustering. The $^{10}\mathrm{Be}(2_3^+)$ state is the particle-hole state in terms of the harmonic oscillator shell-model basis and it is hardly mixed with both the *p*-shell states in the $K^\pi=0_1^+$ and $K^\pi=2^+$ bands in the present results with those interactions. The result of $B(\mathrm{GT})$ for $^{10}\mathrm{Be}(0_1^+)\rightarrow{}^{10}\mathrm{B}(1^+)$ is consistent with the experimental data of the β decay from the mirror nucleus $^{10}\mathrm{C}(0_1^+)\rightarrow{}^{10}\mathrm{B}(1^+)$. In Ref. [7] of the measurements of the strength $B(\mathrm{GT})$, they mentioned about the isospin symmetry violation of β decay strength comparing $B(\mathrm{GT}_-)$ for $^{10}\mathrm{B}(3^+)\rightarrow{}^{10}\mathrm{Be}(2_2^+)$ with $B(\mathrm{GT}_+)$ for the mirror reaction to $^{10}\mathrm{C}$. In the present calculations, we could not find the difference between $B(\mathrm{GT}_-)$ and $B(\mathrm{GT}_+)$ because there is little violation of isospin symmetry between the structures of $^{10}\mathrm{Be}(2_2^+)$ and the mirror state of $^{10}\mathrm{C}$. There exists a significant difference between the excitation energies of the daughter states of $^{10}\mathrm{Be}$ and $^{10}\mathrm{C}$. The present results suggest that the *p*-shell components are dominant in the 2_2^+ states as well as the ground states. The Coulomb energy changes associated with the spatial extent of the states are not so large as to describe the excitation energy difference between the mirror daughter states in this case, though they have been known to be one of the reasons for the energy shift of the mirror states in the case of *sd* orbits in the light nuclei. It is expected that the isospin violation of the wave functions between these mirror states may describe the difference of $B(\mathrm{GT})$ and the excitation energies between the mirror nuclei. We need more detailed investigations to discuss the problem of the isospin symmetry violation of $B(\mathrm{GT})$.

TABLE II. $B(\mathrm{GT})$ of β decays which is the square of the expectation value of the Gamow-Teller operator. The experimental data are the values deduced from the cross sections of $^{10}\mathrm{B}(t,{}^3\mathrm{He})^{10}\mathrm{Be}^*$ at 0° forward angle [7] and the values from [21]. The theoretical values are obtained with case (1) and case (2) interactions for $^{10}\mathrm{Be}$ and $^{10}\mathrm{B}$.

Initial (J^π,E_x) (MeV)	Expt. final (J^π,E_x) (MeV)	$B(\mathrm{GT})$
$^{10}\mathrm{B}(3^+,0)$	$^{10}\mathrm{Be}(2_1^+,3.37)$	0.08± 0.03 (Ref. [7])
$^{10}\mathrm{B}(3^+,0)$	$^{10}\mathrm{Be}(2_2^+,5.96)$	0.95± 0.13 (Ref. [7])
$^{10}\mathrm{B}(3^+,0)$	$^{10}\mathrm{Be}(2^+$ or $3^+,9.4)$	0.31± 0.08 (Ref. [7])
$^{10}\mathrm{C}(0^+,0)$	$^{10}\mathrm{B}(1^+,0.72)$	3.44 (Ref. [21])
	Theory case (1)	
$^{10}\mathrm{B}(3^+)$	$^{10}\mathrm{Be}(2_1^+)$	0.02
	$^{10}\mathrm{Be}(2_2^+)$	1.1
	$^{10}\mathrm{Be}(3_1^+)$	0.40
	$^{10}\mathrm{Be}(4_1^+)$	0.08
	$^{10}\mathrm{Be}(2_3^+)$	0.03
$^{10}\mathrm{Be}(0_1^+)$	$^{10}\mathrm{B}(1^+)$	2.9
	Theory case (2)	
$^{10}\mathrm{B}(3^+)$	$^{10}\mathrm{Be}(2_1^+)$	0.00
	$^{10}\mathrm{Be}(2_2^+)$	0.92
	$^{10}\mathrm{Be}(3_1^+)$	0.38
	$^{10}\mathrm{Be}(4_1^+)$	0.10
	$^{10}\mathrm{Be}(2_3^+)$	0.00
$^{10}\mathrm{Be}(0_1^+)$	$^{10}\mathrm{B}(1^+)$	2.5

V. DISCUSSION

In this section we discuss the structure of the excited states by analyzing the wave functions. Even though the states obtained by VAP mix after the diagonalization of the Hamiltonian matrix, the state $P^{J^\pm}_{MK'}\Phi_{\mathrm{AMD}}(\mathbf{Z}_n^{J^\pm})$ projected from a Slater determinant obtained in VAP with $(J^\pm,K',n)$ is dominant in the final result of the $J_n^\pm$ state. In this section we consider the Slater determinant $\Phi_{\mathrm{AMD}}(\mathbf{Z}_n^{J^\pm})$ as the intrinsic state for the $J_n^\pm$ state.

A. Intrinsic structure

In the excited states, various kinds of structures are found. Here we analyze the structures of the intrinsic states $\Phi_{\mathrm{AMD}}(\mathbf{Z}_n^{J^\pm})$. It is found that the excited levels are classified into rotational bands as 0_1^+, 2_1^+, 4_1^+ states in $K^\pi=0_1^+$ band, 2_2^+, 3_1^+ in $K^\pi=2^+$ band, 0_2^+, 2_3^+, 4_2^+, 6^+ in the second $K^\pi=0_2^+$ band and 1^-, 2^-, 3^-, 4^-, 5^- in $K^\pi=1^-$ band. Particularly the moleculelike states with the well-developed 2α cores construct the rotational bands $K^\pm=0_2^+$ and 1^- in which the level spacing is small because of the large moments of inertia. The density distributions of matter, protons, and neutrons in the intrinsic states $\Phi_{\mathrm{AMD}}(\mathbf{Z}_n^{J^\pm})$ are presented in Fig. 2. We found the $2\alpha+2n$ structures in most of the intrinsic states of the low-lying levels. The structure like $\alpha+t+t$ which has another spatial symmetry may appear in the high energy region above 10 MeV. The density of protons indicates that the clustering structure develops more largely in 1^- than 0_1^+ and most remarkably in 0_2^+. As seen in Fig. 2 the intrinsic structure of the 0_2^+ state has an axial symmetric linear shape with the largest deformation, while the 1^- state has an axial asymmetric shape because of the valence neutrons. The structures of the 0_1^+ and 1_1^- states are similar to the ones of the previous work with the simplest version of AMD [12]. The increase of the degree of the deformation along 0_1^+, 1^-, and 0_2^+ is consistent with the previous works such as [4,6,13]. In the $K^\pm=1^-$ band, the deformation toward the prolate shape shrinks as the total spin J increases.

In the $K^\pi=0_1^+$ band, the 2α cores weaken with the increase of the total spin due to the spin-orbit force. The reduction of the clustering structure is more rapid in the case of interaction (2) with the stronger spin-orbit force, and the 2_1^+ and 4_1^+ states in case (2) interactions contain the dissociation of α. Regarding the dissociation of the α cores, the struc-

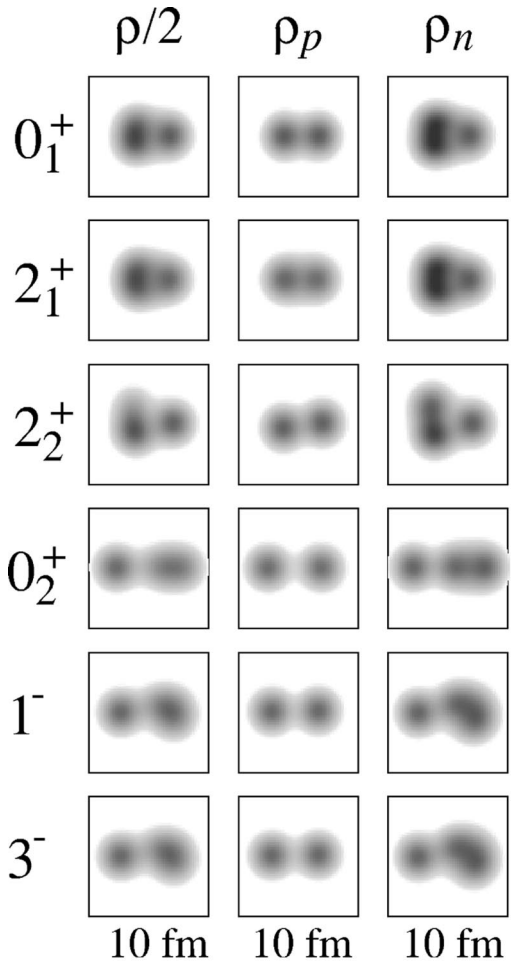

FIG. 2. The density distribution of matter, protons, and neutrons of the intrinsic states are shown at left, middle, and right, respectively. The density is integrated along the axis perpendicular to adequate planes. The figures are for the results with the interaction case (1).

tures of those states are sensitive to the strength of the spin-orbit force.

The 2_3^+ has the remarkably developed moleculelike structure with a linear shape and belongs to the rotational band $K=0_2^+$. On the other hand, the lowest 3^+ state of ^{10}B is the ordinary state in terms of the *p* shell and has the *K* quantum $K=3$. There are differences in the structure and the *K* quantum between the initial and final state. Furthermore, although the energy of 2_3^+ is expected to be close to 2_2^+ in the $K^\pi=2^+$ band, this moleculelike state is hardly mixed by the state with $K=2$. As a result the theory predicts a small value of the Gamow-Teller strength $^{10}\mathrm{B}(3^+)\rightarrow{}^{10}\mathrm{Be}(2_3^+)$.

B. Behavior of valence neutrons

Even though we did not assume the existence of any clusters in the model, we have found the $2\alpha+2n$ structures in most of the intrinsic states as mentioned above. We study the behavior of the valence neutrons surrounding 2α by analyzing the single-particle wave functions to understand the role of the valence neutrons in the neutron-rich Be nuclei. Con-

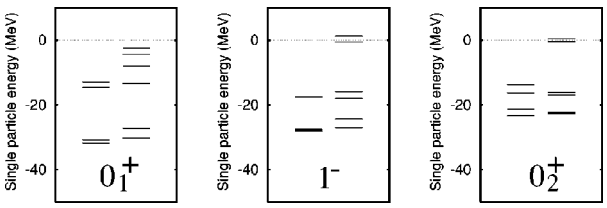

FIG. 3. Single-particle energies in the intrinsic system of the 0_1^+, 1^-, and 0_2^+ states. The energies of protons (neutrons) are displayed in the left (right) side in each figure.

sidering that an intrinsic state is written by a Slater determinant Φ_{AMD}, the single-particle wave functions and the single-particle energies of an intrinsic state are determined by diagonalizing the single-particle Hamiltonian by the analogy with Hartree-Fock theory. First we transform the set of single-particle wave functions φ_i of an AMD wave function into an orthonormal base $\tilde{\varphi}_\alpha$. The single-particle Hamiltonian can be constructed by use of the orthonormal base as follows [4,12]:

$$h_{\alpha\beta}=\langle\tilde{\varphi}_\alpha|\hat{t}|\tilde{\varphi}_\beta\rangle+\sum_{\gamma}^{A}\langle\tilde{\varphi}_\alpha\tilde{\varphi}_\gamma|\hat{v}|\tilde{\varphi}_\beta\tilde{\varphi}_\gamma-\tilde{\varphi}_\gamma\tilde{\varphi}_\beta\rangle$$
$$+\frac{1}{2}\sum_{\gamma,\delta}^{A}\langle\tilde{\varphi}_\alpha\tilde{\varphi}_\gamma\tilde{\varphi}_\delta|\hat{v}_3|\tilde{\varphi}_\beta\tilde{\varphi}_\gamma\tilde{\varphi}_\delta+\tilde{\varphi}_\delta\tilde{\varphi}_\beta\tilde{\varphi}_\gamma+\tilde{\varphi}_\gamma\tilde{\varphi}_\delta\tilde{\varphi}_\beta$$
$$-\tilde{\varphi}_\beta\tilde{\varphi}_\delta\tilde{\varphi}_\gamma-\tilde{\varphi}_\gamma\tilde{\varphi}_\beta\tilde{\varphi}_\delta-\tilde{\varphi}_\delta\tilde{\varphi}_\gamma\tilde{\varphi}_\beta\rangle, \quad (20)$$

where the Hamiltonian operator is written by a sum of the kinetic term, two-body interaction term, and three-body interaction term; $H=\Sigma_i\hat{t}+\Sigma_{i<j}\hat{v}_2+\Sigma_{i<j<k}\hat{v}_3$.

The single-particle energies in the 0_1^+, 1^- and 0_2^+ states are shown in Fig. 3. In each state the neutrons in the four orbits from the bottom correspond to the neutrons in the 2α clusters. The level spacing of these four lower orbits becomes smaller in 1^- than in 0_1^+ and smallest in the 0_2^+ state with the increase of the distance between clusters. We consider the last two neutrons in the higher orbits as valence neutrons surrounding 2α cores. We display the density distributions of single-particle wave functions for the two valence neutrons in the left column of Fig. 4. Figures in the middle and right columns of Fig. 4 are for the normalized density of the positive and the negative parity eigenstates projected from the single-particle wave functions, respectively. By analyzing the single-particle wave functions it is found that two valence neutrons of the 0_1^+ states contain negative parity components of more than 80% (the right column in Fig. 4), which seem to be π bonds [Fig. 5(a)] in terms of molecular orbits. On the other hand, in the case of 0_2^+ band, the last two neutrons are predominantly in the positive parity orbits, which are analogous to the σ bonds [Fig. 5(b)]. In the 1^- band, each valence neutron contains both a positive parity component like σ and a negative parity one similar to π. Since the parity of the total system is negative in the 1^- band, the states after the parity projection have one neutron in the σ orbit and the other neutron in the π orbit. Roughly speaking, the 0_1^+, 1^-, and 0_2^+ states are understood

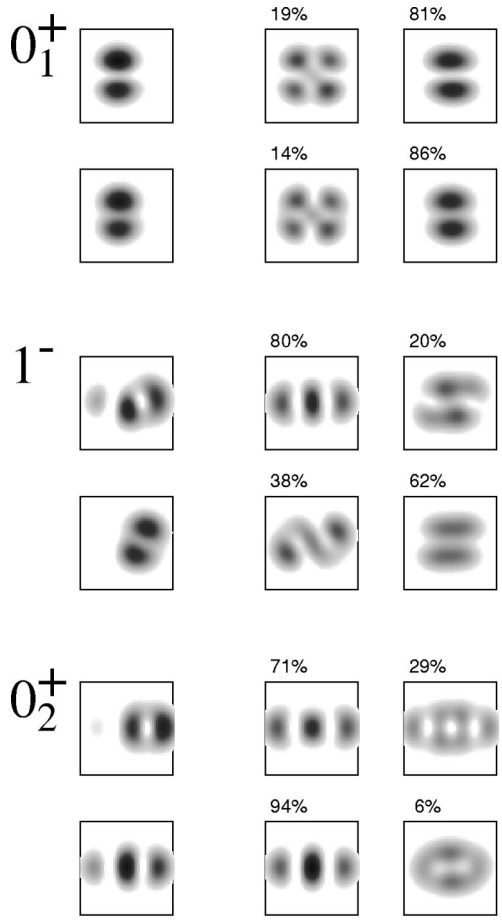

FIG. 4. Density distribution of single-particle wave functions of the valence two neutrons in the intrinsic states of 0_1^+, 1^-, and 0_2^+ (left column). The method for extracting the single-particle wave functions is explained in the text. The middle and right columns are for the density of the positive parity and negative parity components projected from the single-particle wave functions, respectively. The wave functions projected into the parity eigenstates are normalized for presentation.

as 2α and two valence neutrons in π^2, $\sigma\pi$, and σ^2 orbits, respectively. The interesting point is that the valence neutrons play important roles in developing the clustering structure in the excited bands. We can argue that the clustering develops in the 1^- band and mostly in the 0_2^+ band owing to the σ orbits of the valence neutrons, because the σ orbit prefers the prolately deformed system so as to gain its kinetic energy. This idea originates from the application of the two-center shell model to the dimer model for Be isotopes by von

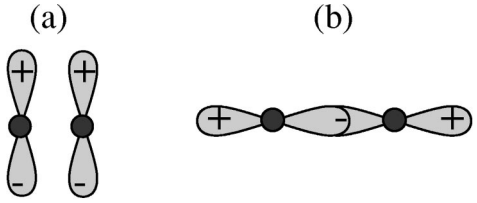

FIG. 5. Schematic figures of the molecular orbits π bond (a) and σ bond (b) surrounding 2α clusters.

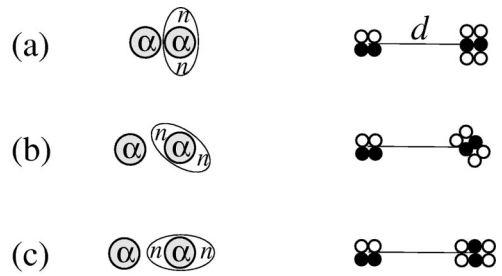

FIG. 6. Schematic figures for the intrinsic structure of 0_1^+, 1^-, and 0_2^+ are shown in the left columns of (a), (b), and (c), respectively. Right columns indicate the three kinds of configurations for the centers of Gaussians in the simplified AMD wave functions which correspond to the two-center ^{6}He$+\alpha$ cluster model for the excited states 0_1^+(a), 1^-(b), and 0_2^+(c) of ^{10}Be. The black (white) circles correspond to the centers of Gaussians of the single-particle wave functions for protons (neutrons).

Oertzen [13] and is consistent with the argument in the work (with the method of AMD+HF) by Doté *et al.* [4].

From the viewpoints of the shell model, the levels $J^\pi = 0_1^+$, 2_1^+, 4_1^+, 2_2^+, and 3_1^+ in the $K^\pi = 0_1^+$ and $K^\pi = 2_1^+$ bands are the *p*-shell states. These states belong to the same [442] spatial symmetry in the supermultiplet limit. On the other hand, the negative parity states in the $K^\pi = 1^-$ are dominated by the $1p$-$1h$ configurations as for the neutron *p* shell. The excited states in the $K^\pi = 0_2^+$ band are particle-hole states where the $2p$-$2h$ configurations with $2\hbar\omega$ excitation are prime. It is consistent with the rotational band seen in the $2\hbar\omega$ states of shell-model calculations [8] and with the 0_2^+ state of Skyrme Hartree-Fock calculations [3]. However, the well developed clustering structures in the $K^\pi = 1^-$ and the $K^\pi = 0_2^+$ bands contain considerably higher configurations which are not included explicitly in the wave function of the $1\hbar\omega$ model space and $(0+2)\hbar\omega$ model space.

C. Mechanism of clustering development

As mentioned above, one of the viewpoints for the mechanism of the clustering development is the moleculelike orbits σ and π. Here we try to understand the mechanism from the other viewpoint of the two-center clustering model.

The reason for the clustering development in the ordinary nuclei has been understood as follows: the system gains the kinetic energy with the development of clustering although it loses potential energy. In order to understand the mechanism of clustering in light unstable nuclei, we think it is helpful to investigate the competition of the kinetic and the potential energies in the moleculelike states of ^{10}Be.

In the density distribution of VAP results, the structures of the 0_1^+, 1^-, and 0_2^+ states seem to be the two-center clustering structures which consist of ^{6}He$+\alpha$ (see Fig. 6). To estimate the dependence of the kinetic and potential energies on the degree of the spatial clustering development we represent the three kinds of configurations for the ^{6}He$+\alpha$ system corresponding to the 0_1^+, 1^-, and 0_2^+ states of ^{10}Be

by the simplified AMD wave functions $\Phi_{\rm AMD}(\mathbf{Z})$ as follows. The intrinsic spin of the single-particle wave functions are fixed to be up or down for simplicity. For the ^{6}He$+\alpha$ system with the intercluster distance d (fm), the centers of single-particle Gaussian wave functions are located around two points $\vec{a}_1=(-3d/5\sqrt{\nu},0,0)$ and $\vec{a}_2=(2d/5\sqrt{\nu},0,0)$. The three kinds of configurations of the centers for 0_1^+, 1^-, and 0_2^+ states are shown in the right figures of Fig. 6. We set the centers for $p\uparrow$, $p\downarrow$, $n\uparrow$, $n\downarrow$ at the point $\vec{a}_1$ and $p\uparrow$, $p\downarrow$ at $\vec{a}_2$. The centers for the last four neutrons are located at the points very close to $\vec{a}_2$ as $\vec{a}_2\pm\vec{\delta}$, where enough small $\vec{\delta}$ is chosen so that the angle θ between $\vec{\delta}$, and $\vec{a}_2$ is $\theta=\pi/2$, $\pi/4$, and 0 corresponding to the 0_1^+, 1^-, and 0_2^+ states, respectively. For the parity eigenstates projected from these three kinds of the simplified AMD wave functions $\Phi_{\rm AMD}(\mathbf{Z})$, we calculate the expectation values of total, kinetic, and potential energies as the function of the intercluster distance d:

$$\langle H\rangle\equiv\frac{\langle(1\pm P)\Phi_{\rm AMD}(\mathbf{Z})|H|(1\pm P)\Phi_{\rm AMD}(\mathbf{Z})\rangle}{\langle(1\pm P)\Phi_{\rm AMD}(\mathbf{Z})|(1\pm P)\Phi_{\rm AMD}(\mathbf{Z})\rangle}, \quad (21)$$

$$\langle T\rangle\equiv\frac{\langle(1\pm P)\Phi_{\rm AMD}(\mathbf{Z})|T|(1\pm P)\Phi_{\rm AMD}(\mathbf{Z})\rangle}{\langle(1\pm P)\Phi_{\rm AMD}(\mathbf{Z})|(1\pm P)\Phi_{\rm AMD}(\mathbf{Z})\rangle}, \quad (22)$$

$$\langle V\rangle\equiv\frac{\langle(1\pm P)\Phi_{\rm AMD}(\mathbf{Z})|V|(1\pm P)\Phi_{\rm AMD}(\mathbf{Z})\rangle}{\langle(1\pm P)\Phi_{\rm AMD}(\mathbf{Z})|(1\pm P)\Phi_{\rm AMD}(\mathbf{Z})\rangle}, \quad (23)$$

where we omit the spin-orbit and the Coulomb forces for simplicity. In Fig. 7 we present the total energy, the kinetic energy, and the potential energy for the three kinds of clustering states 0_1^+, 1^-, and 0_2^+ as the function of the distance d between ^{6}He and α clusters. As shown in the figure for the total energy $\langle H\rangle$, the optimum distances indicate that the clustering structure develops in the system for the 1^- state and is most remarkable in the state for 0_2^+, which is consistent with the present results of VAP calculations. The shift of the minimum point of the total energy is understood by the energetic advantage of the kinetic part as follows. It is found that the kinetic energies in the small-d region are sensitive to the configurations, while in the case of the potential energies significant differences are not seen in the three configurations. When the clusters approach each other the kinetic energy in the configuration for the 1^- state becomes larger than 0_1^+ by $1/2\hbar\omega$ (about 7 MeV for $\nu=0.17$), because all the neutrons in 0_1^+ are in $0s$ and $0p$ shells, while in the negative parity state for 1^- one valence neutron must rise to the higher sd shell in the small-d region. Since in the small-d limit the wave function is almost the the same as the harmonic oscillator shell-model wave function due to the antisymmetrization, the kinetic energy of the sd shell is larger than by $1/2\hbar\omega$ the one of the p shell. Thus the system for 1^- loses the energy in the small distance d, as a result, the minimum point of the total energy shifts to the larger d region than the case of the 0_1^+ state. In the case of the linear configuration for the excited 0_2^+ state, the two valence neutrons occupy the sd orbit in the small-d limit and the kinetic energy is larger than 0_1^+ by $\hbar\omega$. That is why the optimum point d in 0_2^+ is the largest of the three. In other words, when the clusters approach each other, the system feels the repulsive force in the kinetic part because of the Pauli principle. That is the reason why the clustering structure remarkably develops in the 0_2^+ state. In the analysis with this simplified two-cluster model, we can conclude that the clustering develops so as to gain the kinetic energy. It is compatible with the viewpoint of the molecular σ orbit.

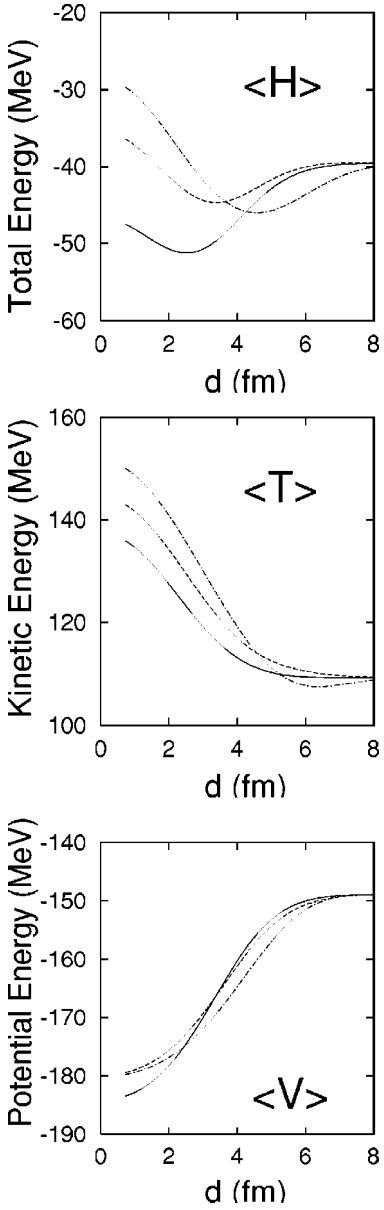

FIG. 7. Total, kinetic, and potential energies as the distance between clusters in the simplified ^{6}He$+\alpha$ cluster models for the excited states of ^{10}Be. The adopted interaction is the MV1 force with $m=0.62$, and the spin-orbit and the Coulomb forces are omitted. The distance d between clusters and the configuration for the 0_1^+, 1^-, and 0_2^+ states are defined in the text. The solid lines, dashed lines, and dot-dashed lines correspond to the energies in the system for 0_1^+, 1^-, and 0_2^+ states of ^{10}Be, respectively.

VI. SUMMARY

We studied the structures of excited states of ^{10}Be by performing variational calculations after the spin-parity projection in the framework of antisymmetrized molecular-dynamics (AMD). We explained the formulation of the variation after projection and the method to construct the higher excited states with AMD.

The excitation energies of many levels of ^{10}Be were reproduced by AMD calculations with the finite range interactions. The theoretical results agree well with the experimental data of $E1$, $E2$ transition strength. The results successfully describe the new data of B(GT) for the β transition strength reduced from the 0° angle cross sections of the charge exchange reactions ^{10}B$(t,{}^3$He$)^{10}$Be*.

In the present work on ^{10}Be we tried a few sets of the interaction parameters, however, there remains ambiguity in choosing the parameters such as the strength of the Majorana exchange force and the strength of the spin-orbit force. In order to determine these parameters we should examine many data for neighboring nuclei systematically.

We discuss the structures of excited states. By analyzing the intrinsic structures it is found that the excited levels are classified into the rotational bands as $K^\pi=0_1^+$, 2^+, 0_2^+, and 1^-. Although the α clusters are not assumed in the model, the theoretical results show that the $2\alpha+2n$ structures appear in most of the states. Particularly the molecularlike states with the developed 2α structure constructs the rotational bands $K^\pi=0_2^+$ and 1^- in which the level spacing is small because of the large deformations. The moleculelike structure develops more largely in $K^\pi=1^-$ than in $K^\pi=0_1^+$ and most remarkably in $K^\pi=0_2^+$.

We extracted the single-particle wave functions to discuss the behavior of the valence neutrons. In the analysis of the intrinsic states of 0_1^+, 1^-, and 0_2^+ states (the bandheads of the rotational bands $K^\pi=0_1^+,1^-,0_2^+$), we found that the two valence neutrons are in the molecular orbits surrounding 2α. The positive and negative parts of the orbits are analogous to the σ and π bonds in terms of the electron orbits in molecules. Roughly speaking, the 0_1^+ states, 1^- and 0_2^+ bands are regarded as the states with the two valence neutrons in π^2, $\sigma\pi$, and σ^2 orbits, respectively. The neutrons in the σ orbit play an important role for the development of clustering because the σ orbit profits from the kinetic energy in the prolately deformed system.

In order to understand the mechanism of the clustering development in the excited states of ^{10}Be, we analyze the kinetic and the potential parts of the total energies with the simplified model of the two-center ^{6}He$+\alpha$ cluster model. In the 1^- and 0_2^+ states, when the distance between clusters becomes small the systems feel the repulsive kinetic energy because the valence neutrons must rise into higher orbits. Because of the repulsive kinetic energy in the small intercluster distance the clustering structure develops in the excited states 1^- and 0_2^+ to gain the kinetic energy.

ACKNOWLEDGMENTS

The authors would like to thank Dr. N. Itagaki for many discussions. They are also thankful to Professor W. Von Oertzen for helpful discussions and comments. The valuable comments of Professor M. Fujiwara are also acknowledged. The computational calculations of this work were supported by the Research Center for Nuclear Physics in Osaka University, the Yukawa Institute for Theoretical Physics in Kyoto University, and the Institute of Physical and Chemical Research.

[1] M. Seya, M. Kohno, and S. Nagata, Prog. Theor. Phys. **65**, 204 (1981).
[2] Y. Kanada-En'yo, A. Ono, and H. Horiuchi, Phys. Rev. C **52**, 628 (1995); Y. Kanada-En'yo and H. Horiuchi, *ibid.* **52**, 647 (1995).
[3] S. Takami, K. Yabana, and K. Ikeda, Prog. Theor. Phys. **96**, 407 (1996); **94**, 1011 (1995).
[4] A. Doté, H. Horiuchi, and Y. Kanada-En'yo, Phys. Rev. C **56**, 1844 (1997).
[5] N. Itagaki and S. Okabe, preprint RIKEN-AF-NP-314 (1999).
[6] Y. Ogawa (private communications).
[7] I. Daito *et al.*, Phys. Lett. B **418**, 27 (1998).
[8] E. K. Warburton and B. A. Brown, Phys. Rev. C **46**, 923 (1992).
[9] A. A. Wolters, A. G. M. van Hees, and P. W. M. Glaudemans, Phys. Rev. C **42**, 2062 (1990).
[10] H. Nakada and T. Otsuka, Phys. Rev. C **49**, 886 (1994).
[11] P. Navrátil and B. R. Barrett, Phys. Rev. C **57**, 3119 (1998).
[12] Y. Kanada-En'yo, Ph.D. thesis, Kyoto University, 1996.
[13] W. von Oertzen, Z. Phys. A **354**, 37 (1996).
[14] Y. Kanada-En'yo and H. Horiuchi, Prog. Theor. Phys. **93**, 115 (1995).
[15] Y. Kanada-En'yo, Phys. Rev. Lett. **81**, 5291 (1998).
[16] Y. Kanada-En'yo, H. Horiuchi, and A. Doté, J. Phys. G **24**, 1499 (1998).
[17] T. Ando, K. Ikeda, and A. Tohsaki, Prog. Theor. Phys. **64**, 1608 (1980).
[18] N. Yamaguchi, T. Kasahara, S. Nagata, and Y. Akaishi, Prog. Theor. Phys. **62**, 1018 (1979); R. Tamagaki, *ibid.* **39**, 91 (1968).
[19] Y. Kanada-En'yo and H. Horiuchi, Phys. Rev. C **55**, 2860 (1997).
[20] F. Ajzenberg-Selove, Nucl. Phys. **A490**, 1 (1988).
[21] W.-T. Chou, E. K. Warburton, and B. A. Brown, Phys. Rev. C **47**, 163 (1993).